www.sciencemag.org/content/353/6304/1123/suppl/DC1

Supplementary Materials for

Identification of an elaborate complex mediating postsynaptic inhibition

Akiyoshi Uezu, Daniel J. Kanak, Tyler W.A. Bradshaw, Christina M. Catavero, Alain C. Burette, Richard J. Weinberg, Scott H. Soderling

*Corresponding author. Email: scott.soderling@duke.edu

Published 9 September 2016, *Science* **353**, 1123 (2016)
DOI: 10.1126/science.aag0821

This PDF file includes

Other Supplementary Material for this manuscript includes the following:
(available at www.sciencemag.org/content/353/6304/1123/suppl/DC1)

Tables S1 to S6 as Excel files

Supplemental Text: Discussion

Our results finding 27 proteins implicated in seizure susceptibility/familial epilepsy, ID, or autism suggest the iPSD is a site of burden for brain disorders. While several of these are known to regulate GABAergic synaptic transmission (in particular $GABA_AR$ subunits), many are new components of the iPSD. Of the newly-defined iPSD proteins implicated in developmental disorders, many are signaling proteins or are proteins of unknown functions. Examples of signaling proteins enriched at the iPSD and implicated in brain disorders include: PX-RICS, a Rho-family GAP protein implicated in the autism associated Jacobsen Syndrome (*43*); IQSEC2, an Arf-GEF implicated in epileptic encephalopathies (*44*); Cdkl5, a kinase whose mutations cause early infantile epileptic encephalopathy-2 (*45, 46*); Tbc1d24, a potential Arf GTPase effector in which mutations cause familial infantile myoclonic epilepsy (*47, 48*); and GNAQ, which encodes the signaling protein $G_{\alpha q}$ whose activating mutations are linked to Sturge-Weber Syndrome characterized in part by seizures and ID (*49*). iPSD proteins genetically coupled with developmental brain disorders, but of unknown function include: GSE1, a coiled-coiled domain protein whose duplication is associated with cognitive deficits and epilepsy (*50*); cc2d1a, a calcium binding protein implicated in severe ID (*51*); and Rogdi, multiple mutations of which cause Kohlschütter-Tönz syndrome (KTS), an autosomal-recessive disorder characterized by the combination of epilepsy and psychomotor regression (*52, 53*). Interestingly, cc2d1a null mice exhibit altered mIPSCs during development and die shortly after birth due to an inability to breathe and swallow, a phenotype that overlaps with gephyrin knockout mice (*54*). Moreover, several other iPSD proteins we identified are associated with seizure susceptibility when genetically ablated in mice. These proteins include: the transmembrane adhesion protein, Elfn1 (*55*); the clathrin adaptor protein, Ap3m2 (*56*); and the $GABA_AR$ interacting ubiquitin ligase, Trim3 (*39*). Together, the localization of these proteins to the iPSD reveals new insights into how mutations of these genes may ultimately result in pathology by directly altering neuronal inhibition.

Materials and Methods

Animals

C57BL/6J (stock no. 000664) and Rosa26-LSL-Cas9 knockin (stock No. 026175) mice were purchased from Jackson Laboratory. All mice were housed (3–5 mice per cage) in the Duke University's Division of Laboratory Animal Resources facilities. All procedures were conducted with a protocol approved by the Duke University Institutional Animal Care and Use Committee in accordance with US National Institutes of Health guidelines.

Plasmid construction and AAV production

HA-InSyn1 (NM_176921), HA-InSyn2 (NM_001143802) and myc-PX-RICS expression constructs were made by subcloning each cDNA along with epitope tags into the pBetaActin plasmid (*57*). Myc-PX-RICS, Flag-IQSEC3 and pCAGZreg Geph.FingR:eGFP were provided from T. Nakamura (University of Tokyo), H. Sakagami (Kitasato University) and D. Arnold (University of Southern California), respectively. CRISPR constructs were made by cloning each gRNA sequence into px458 (Addgene; 48138), (InSyn1#12; ATTCGGGGTGCCCCGGACCT, InSyn1#17; ATGGTCATCGGGCAACTTGA, $GABA_AR\gamma2$;

CTCCTGCTATCGCTCTACCCAGG, InSyn2#46; GATCTGCCGGTTAGGGTCGA, InSyn2#50; GATATGCCCTCGACCCTAAC). CRISPR resistant HA-InSyn1 and HA-InSyn2 constructs were generated by introducing mutation inside the gRNA targeting sites into the cDNA expression constructs (InSyn1; GATCTGCCGGTTAGGATCAAGTG, InSyn2; GATGGTCATAGGCCAGCTCGAGGG). BirA-gephyrin was generated by cloning BirA (Addgene 36047) into NheI/XhoI sites of pCMV-EGFP-gephyrin (M. Kneussel, University of Hamburg, Germany)) using In-Fusion cloning (Clontech) to replace EGFP. AAV expressing BirA-gephyrin construct (pAAV-BirA-gephyrin) was made with 4 amplicons (human synapsinI promoter, BirA-gephyrin, WPRE and BGHpolyA) ligated into AAV9.EF1α.DIO.ArpC3-P2A-eGFP.WPRE (*58*) NotI sites by In-Fusion. PSD-95–BirA was made by cloning BirA into pCMV-PSD-95–EGFP (Cagla Eroglu, Duke University) between EcoRI and XhoI sites to replace EGFP. pAAV–PSD-95–BirA, pAAV-BirA , pAAV-synI-InSyn1-GFP or pAAV-synI-GFP was generated replacing with BirA-gephyrin of pAAV-BirA-gephyrin between SalI and EcoRI sites. pAAV-U6-sgRNA-hSyn-Cre was produced by removing Cre-2A-eGFP-KASH with KpnI/EcoRI digestion of AAV-U6-sgRNA-hSyn-Cre-2A-eGFP-KASH and cloning Cre cDNA back into the plasmid. For AAV purification, HEK293T cells were cultured in DMEM containing 10% fetal bovine. 1.5 x10^7 HEK293T cells per 15cm dish were plated one day before transfection for a total of six dishes per virus. Next day, cells were transfected with 30ug pAd-DELTA F6, 15 µg serotype plasmid AAV2/9, and 15ug AAV plasmid with PEI MAX. 18 hours later, medium was replaced with 20ml DMEM + 10% FBS. 48 hours later, cells were collected and centrifuged at 1200 rpm for five minutes at room temperature. The final cell pellet was resuspended in 4ml of cell lysis buffer (15mM NaCl, 5mM Tris-HCl, pH 8.5) and freeze-thawed three times in a dry ice-ethanol bath and 37°C water bath. 50U/ml Benzonase was added to the cell lysate which was then incubated in a 37°C water bath for 30 minutes, and centrifuged at 4500 rpm for 30 minutes at 4°C. Supernatant was added over gradient of 15%, 25%, 40% and 60% iodixanol solution and centrifuged using a Beckman Ti-70 rotor, spun at 67,000 rpm for one hour. The viral solution was washed with 1X PBS three times and concentrated to 200 µl using a 100 kDa filter. Some of the AAVs were also produced by the University of Pennsylvania Vector Core. Aliquots were stored at –80°C until use.

In vivo BioID (iBioID)

Each AAV BirA probe virus was injected into C57/B6J mouse brain, mainly into hippocampus and the cortex at P0 to P2. After 24 to 35 days post virus injection, biotin was subcutaneously injected at 24 mg/kg for 7 consecutive days to increase the biotinylation efficiency. For each BirA probe, 6-8 mice were used for each biotinylated protein purification and each purification was performed independently at least 3 times. After each cortex and hippocampus was Dounce homogenized 15 times with 300 µL of buffer-A (50 mM HEPES pH 7.5, 150 mM NaCl, 1mM EDTA supplemented with 2mM AEBSF, 4ug/mL Leupeptin and 4ug/mL PepstatinA), an equal volume of buffer-B (50mM HEPES pH7.5, 150mM NaCl, 1mM EDTA, 0.4% SDS, 2% TritonX-100, 2% deoxycholate) was added. The lysed samples were then sonicated twice for 10 seconds each and centrifuged at 15,000 g for 15min at 4° C. Supernatant was further ultracentrifuged at 100,000g for 30min at 4C. SDS was added to the cleared supernatant to a final concentration of 1% and heated at 95C for 5 min. Sample was cooled on ice and incubated with 20 µL of NeutrAvidin Agarose at 4° C for 16 hrs. Beads were washed twice with 2% SDS, twice with 1% TritonX-100, 1% deoxycholate, 25 mM LiCl, twice with 1M NaCl and 5 times with 50 mM ammonium bicarbonate. Bound proteins were eluted in 0.1% RapiGest SF Surfactant, 2mM

biotin, 50mM ammonium bicarbonate solution at 60° C for 2 hrs. The eluted sample was depleted with anti HA antibody conjugated agarose for 4 hrs at 4C followed by additional incubation with anti-pyruvate carboxylase antibody (clone 3H2AD9, life technologies) conjugated with agarose for 4hrs. Samples were then dialyzed against excess amount of 50 mM ammonium bicarbonate for 3-4 hrs twice. The final protein concentration was measured by BCA.

Affinity Purification for MS

AAV expressing InSyn1-GFP or GFP alone were injected into mouse brain at P0. After decapitated at P40, the hippocampus and the cortex were quickly dissected and homogenized (25 mM HEPES pH 7.5, 150 mM NaCl, 1 mM EDTA, 1% NP-40, 5mM NaF, 1mM orthovanadate, 1 mM AEBSF, 2ug/mL Leupeptin and 2 µg/mL PepstatinA). Samples were cleared at 15,000g, 15 min with additional centrifugation of 100,000g, 30min. Lysates were incubated with GFP-Trap overnight followed by 4 washes with the same buffer except containing 500mM NaCl. After additional washes with 50 mM ammonium bicarbonate, pulldown-samples were directly trypsinized and subjected to MS analysis.

Liquid Chromatography and Semi-quantitative Mass Spectrometry Analysis of Biotinylated Proteins

Proteins eluted from Streptavidin resin in 50 mM ammonium bicarbonate, pH 8 were supplemented with Rapigest SF surfactant to 0.1% prior to being reduced with 10 mM dithiolthreitol and alkylated with 20 mM iodoacetamide. In-solution trypsin digestion was accomplished by the addition of 200 ng trypsin incubated for 18 hr at 37° C. Samples were then acidified to hydrolyze Rapigest prior to lyophilization. Prior to LC/LC-MS analysis, samples were resuspended in 15 µL of 2% acetonitrile/1% TFA supplemented with 10 fmol/µL yeast ADH. Qualitative two-dimensional liquid chromatography–tandem mass spectrometry (LC/LC-MS/MS) utilized a high-low pH reversed-phase/reversed-phase configuration on a nanoAcquity UPLC/UPLC system coupled to a Synapt G2 HDMS mass spectrometer with nanoelectrospray ionization. Briefly, 5 µL of each sample was injected at 2 µL/min onto a 5 µm XBridge BEH130 C18 300 µm × 50 mm column at 97/3 v/v water/MeCN in 20 mM ammonium formate (pH 10). Peptides were eluted at 2 µL/min in five steps of 10.8%, 14.0%, 16.7%, 20.4% and 50.0% MeCN, and each of these fractions were separately diluted 10-fold online with 99.8/0.1/0.1 v/v/v water/MeCN/formic acid and trapped on a 5 µm Symmetry C18 180 µm × 20 mm column, followed by second dimension separations were performed on a 1.7 µm Acquity BEH130 C18 75 µm × 150 mm column using a linear gradient of 7 to 35% MeCN with 0.1% formic acid over 37 min, at a flow rate of 0.5 µL/min and column temperature of 35 °C. Data collection was performed in ion-mobility-assisted data-independent acquisition (HDMSE) modes. HDMSE used a 0.6 s alternating cycle time between low (6 V) and high (27–50 V) collision energy (CE). Raw LC-MS/MS data files were processed in Protein Lynx Global Server against a SwissProt database (*Mus musculus* taxonomy) containing both forward and reverse entries of each protein (16,547 forward entries). Search tolerances were 10 ppm for precursor ions and 0.04 Da for product ions using trypsin specificity with up to two missed cleavages. Carbamidomethylation (+57.0214 Da on C) was set as a fixed modification, whereas oxidation (+15.9949 Da on M) and deamidation (+0.98 Da on N and Q were searched as a differential mass modification. All searched spectra were imported into Scaffold and scoring thresholds were set to achieve a protein false discovery rate of 0.3% and a peptide false discovery rate of 0.1% using the PeptideProphet algorithm. The iBAQ method was utilized to score a protein's abundance in a relevant biological

fraction. Briefly, iBAQ was calculated by the sum of a proteins spectral counts divided by the predicted number of tryptic peptides calculated *in silico*. iBAQ scores were normalized (divided by the sum of iBAQ scores in a particular biological fraction), and finally scaled (set maximum to 1,000) in order to account for exclusive hits. In order to prioritize top hits, enrichment relative to the BirA fraction was calculated. Proteins with a log base 2 fold change greater than 2.0 (PSD-95–BirA iBAQ) or 2.5 (BirA-Gephyrin and InSyn1-GFP iBAQ) were considered top hits.

Liquid Chromatography and Quantitative Mass Spectrometry Analysis of Biotinylated Proteins

Proteins eluted from the Streptavidin resin were lyophilized to dryness and resuspended in 20 uL of 1X LDS loading buffer supplemented with 10 mM dithiolthreitol. All 20 µL was loaded onto an Invitrogen NuPAGE 4-12% SDS-PAGE gel and run for approximately 5 min to electrophorese all proteins into the gel matrix. The entire MW range was then excised in a single gel-band and subjected to standardized in-gel reduction, alkylation, and tryptic digestion. Following lyophilization of the extracted peptide mixtures, samples were resuspended in 12 µL of 2% acetonitrile/1% TFA supplemented with 10 fmol/uL yeast ADH. From each sample, 3 µL was removed to create a QC Pool sample which was run periodically throughout the acquisition period. Quantitative LC/MS/MS was performed on 3 µL of each sample, using a nanoAcquity UPLC system coupled to a Thermo QExactive Plus high-resolution accurate mass tandem mass spectrometer via a nanoelectrospray ionization source. Briefly, the sample was first trapped on a Symmetry C18 20 mm × 180 µm trapping column (5 µL/min at 99.9/0.1 v/v water/acetonitrile), after which the analytical separation was performed using a 1.7 µm Acquity BEH130 C18 75 mm × 250 mm column with a 90-min linear gradient of 5 to 40% acetonitrile with 0.1% formic acid at a flow rate of 400 nanoliters/minute (nL/min) with a column temperature of 55C. Data collection on the QExactive Plus mass spectrometer was performed in a data-dependent acquisition (DDA) mode of acquisition with a r=70,000 (at m/z 200) full MS scan from m/z 375 – 1600 with a target AGC value of 1e6 ions followed by 10 MS/MS scans at r-17,500 (at m/z 200) at a target AGC value of 5e4 ions. A 20 s dynamic exclusion was employed to increase depth of coverage. Following the 17 LC-MS/MS analyses, data was imported into Rosetta Elucidator v3.3, and all LC-MS/MS runs were aligned based on the accurate mass and retention time of detected ions ("features") which contained MS/MS spectra using PeakTeller algorithm. The relative peptide abundance was calculated based on area-under-the-curve (AUC) of aligned features across all runs. The overall dataset had 249,993 quantified isotope (peptide) groups. Additionally, 562,121 MS/MS spectra were acquired for peptide sequencing by database searching. This MS/MS data was searched against a SwissProt_Mouse database which also contained a reversed-sequence "decoy" database for false positive rate determination. Database searching was performed within Mascot Server and then subjected to peptide/protein teller algorithm within Rosetta Elucidator to annotate the data at a ~0.9% peptide level FDR. Searching allowed variable M (oxidation, +16 Da) and NQ (deamidation, +1 Da) modifications. Carbamidomethylation on C (alkylation, +57 Da) was considered static modifications. To generate protein expression values, all features associated with a protein were summed to the protein level, with the same set of features being used in all individual LC-MS/MS analysis. To account for subtle variations in IP efficiency, all features associated with Propionyl-CoA carboxylase alpha and beta chain as well as all features associate with human keratin were removed and the remaining features were subjected to a robust mean (excluding the highest and lowest 10% of the signals) normalization. The average quantitative value for a protein was calculated for bait and control from three biological replicates. Proteins with a fold enrichment

greater than 2.5 bait versus BirA alone were considered enriched. To generate a high confidence list of hits, intermediate filaments or proteins known to reside at other subcellular sites based on EM immunostaining of non-specific immunostaining (Fig. S1A) (mitochondria, nucleus, secreted, carboxylases) were manually filtered (Table S1) as likely artifacts of overexpression or endogenously biotinylated proteins. Proteins significantly enriched in BirA versus any other bait were also excluded from all fractions. Student's T-test was used to assess significance of log base 2 transformed protein quantitative values compared to control. Proteins with a p-value less than 0.05 were considered significant.

Protein Networks Analysis

Network figures were created using Cytoscape (v3.2), with nodes corresponding to the gene name (multiple isoforms of proteins were collapsed into one node based on gene nomenclature) for proteins identified in the proteomic analysis. A non-redundant list of protein-protein interactions was assembled using GeneMania, BioGRID (v3.4.134), and STRING. In all networks, node size is proportional to fold enrichment over BirA alone. However, in iBAQ networks, the bait (Gephyrin, PSD-95, InSyn1) node sizes were set manually. In the iPSD network, node size is proportional to composite fold enrichment or sum of gephyrin, collybistin, and InSyn1 fold enrichment values for proteins enriched in more than one iPSD bait fraction. Clustergrams were created by manual inspection based on uniprot database annotation and literature review.

Electron Microscopy

Briefly, deeply-anesthetized mice were perfused with an aldehyde mixture (either 0.1% glutaraldehyde and 4% depolymerized paraformaldehyde, or 2% glutaraldehyde and 2% paraformaldehyde, dissolved in 0.1 M phosphate buffer, pH 7.4); brains were removed and postfixed overnight at 4 °C in the same fixative. Fifty micrometer-thick sections were cut on a Vibratome for histochemistry. We used tagged streptavidin to identify biotinylated sites. Tissue permeabilized by freeze-thaw after cryoprotection in 30% sucrose was treated with sodium borohydride (to mask free aldehyde binding sites), then incubated overnight on a shaker with streptavidin conjugated with streptavidin conjugated to Cy-3 for immunofluorescence. After reaction, sections were collected on microscope slides and coverslipped with antifade medium, prior to examination with standard epifluorescence optics. For electron microscopy, we used streptavidin conjugated to Nanogold or to horseradish peroxidase. To visualize the gold label, we used a silver intensification kit (IntenSE M); for HRP we used a standard nickel-diaminobenzidine reaction. Sections were rinsed and contrasted with 0.5% osmium tetroxide for 30 minutes. After rinse in maleate buffer (0.1 M pH 6.0), sections were stained en bloc with 1% uranyl acetate, then dehydrated, infiltrated with Epon-Spurr resin, flat-embedded between sheets of Aclar plastic, and allowed to polymerize for 2 days at 60°C. Chips of interest were prepared from the tissue sections, glued to plastic blocks, cut on an ultramicrotome and collected on copper mesh grids. To identify GABAergic profiles, thin plastic sections were collected on nickel grids; postembedding immunogold staining was performed using a Sigma anti-GABA antibody at 1:10K dilution. Grids were examined with a Tecnai 12 TEM operating at 80 KV.

Organotypic hippocampal slice preparation

Slice cultures from mouse hippocampus were prepared as described previously (*59*). Briefly p6 pups deeply anesthetized with isoflurane were decapitated; the hippocampus was rapidly

dissected into medium containing the following (in mM): HEPES (25), $NaHCO_3$ (2), sucrose (248), glucose (10), KCl (4), $MgCl_2$ (5), $CaCl_2$ (1). Then, 350 μm slices were cut with a tissue chopper and transferred to the surface of 0.4μm pore size membrane inserts placed in culture media containing the following (in mM): L-glutamine (1), CaCl2 (1), $MgSO_4$ (2), D-glucose (12.9), $NaHCO_3$ (5.2), HEPES (25), insulin 1μg/mL, ascorbic acid 0.075%, heat-inactivated horse serum 20%, HEPES-based MEM 8.4 g/L. The pH was adjusted to 7.35 with 1 N NaOH and osmolarity was adjusted to 290 Osm. Slice-containing plates were maintained in a 37°C incubator with 5% CO_2. Three days after incubation, cultures were transfected biolistically with a gene gun. Bullets were prepared with 12 μg of CRISPR constructs and 6 mg of 1.6 μm gold particles. Synaptic current recordings were performed between 3 and 4 weeks after transfection as previously described (*15*). To re-express InSyn1 or InSyn2, gRNA resistant expression plasmids were co-transfected along with CRISPR constructs. For staining, slices were fixed with 4% PFA/4% sucrose in 1 x PBS for 15min at 37C followed by 1% Triton X-100 in 1 x PBS incubation overnight at 4°C. Tissues were removed from the membrane and treated with 0.2% Triton X-100/5% normal goat serum in 1 x PBS for 2hrs at RT then incubated with primary antibodies; rabbit anti-VGAT (Synaptic systems 131002; 1:1000), guinea pig anti-VGLUT1 (Millipore AB5905; 1:2000), mouse anti-HA (covance HA.11; 1:500), Alexa-680 conjugated streptavidin (Jackson 016-620-084; 1:500) at 4C for 3 overnights. After 3 times washes with PBS containing 0.2% Triton X-100, tissues were stained by species matched secondary antibodies; goat anti-mouse Alexa 488 (LT A11001; 1:500), goat anti-rabbit Alexa 555 (LT A21428; 1:500), goat anti-guinea pig Alexa 555 (LT A21435; 1:500) and Alexa-680 conjugated streptavidin (1:500) overnight at 4°C. To pulldown biotinylated proteins, slices were infected with AAV:BirA, AAV:PSD-95–BirA or AAV:gephyrin-BirA at DIV2 (days in vitro) and 100 μM biotin was added from DIV11 to 12. Tissues (4 slices) were removed and lysed in 400 μL of RIPA buffer (150 mM NaCl, 20 mM Tris/Cl pH7.5, 0.1%SDS, 0.1%TritonX100, 1% deoxycolate, 1mM EDTA supplemented with 2 mM AEBSF, 4 μg/mL Leupeptin and 4 μg/mL PepstatinA). After brief sonication, samples were centrifuged 15,000g for 15 min at 4C. Supernatants were incubated with 10 μL of avidin agarose for 24 hrs at 4C followed by washing 3 times with RIPA buffer except with 1M NaCl. Proteins were eluted by Laemmli sample buffer containing 1 mM biotin.

Anti InSyn1 antibody production

We raised a rabbit antibody against full-length InSyn1 recombinant protein and affinity purified as described previously (*60*).

Immunoblotting

Equal amounts of protein were loaded on 4-20% or 10% polyacrylamide gels. The proteins were separated by SDS-PAGE, blotted onto nitrocellulose membrane and incubated with appropriate primary antibodies; mouse anti-collybistin (BD 612076; 1:2500), mouse anti-NR2B (BD 610417; 1:1000), rabbit anti-GluR1 (Abcam ab31232; 1:1000), followed with species matched secondary antibodies either with HRP conjugated (GE NA931, NA934; 1:5000) or infrared dye conjugated (LI-COR 926-32211, 926-68070; 1:5000).

Single-Cell Electrophysiology

We recorded whole-cell currents from the soma of CA1 pyramidal cells using 2-4 MΩ borosilicate glass micropipettes with silver-silver/chloride electrodes. Miniature inhibitory

postsynaptic currents (mIPSCs) were recorded at –55 mV holding potentials; intracellular solution contained (in mM): KCl (130), HEPES (10), NaCl (5), QX-314 (5), MgATP (4), EGTA (1); 300-310 mOsm; pH adjusted to 7.3-7.4 with KOH. The extracellular solution contained (in mM): NaCl (124), $NaHCO_3$ (26), dextrose (10), $CaCl_2$ (2), KCl (3), $MgS0_4$ (1.3), NaH_2PO4 (1.25), D-APV (0.05), CNQX (0.02), and TTX (0.001), 294-297 mOsm; continuously bubbled at room temperature (24 °C) with 95:5 O_2:CO_2 (carbogen). AMPA-mediated miniature excitatory postsynaptic currents (AMPA-mEPSCs) were recorded at –70 mV holding potentials; the intracellular solution contained (in mM): Cs-methansulfonate (135), HEPES (10), phosphocreatine (10), NaCl (8), TEA-Cl (5), QX-314 (5), MgATP (4), EGTA (0.3), and Na_2GTP (0.3); 305-310 mOsm; pH adjusted to 7.3-7.4 with CsOH. The extracellular solution was as above without CNQX along with the following modifications: $CaCl_2$ (4), picrotoxin (0.1), bicuculline methiodide (0.001), and warmed to 27.5 °C. Signals were not corrected for the estimated liquid-liquid junction potentials, –3.6 mV (mIPSC) and 8.50 mV (mEPSC). Recordings commenced 5-10 minutes (mIPSCs) or 10-15 minutes (mEPSCs) after rupturing Giga-Ohm seals (1-10 MΩ). Throughout the experiments, we monitored series resistance and leak current from membrane current responses elicited by 300 ms, –5 mV step potentials. We also monitored current amplitude and frequency stability using a custom detection algorithm written MATLAB. Acquisition was controlled in the Clampex software environment using a Multiclamp 700B amplifier and Digidata 1550 analog-to-digital converter. Signals were low-pass filtered at 3 kHz, amplified at 10x gain, and digitized at 50 kHz for storage on a computer hard drive. Currents were manually detected offline in MiniAnalysis using detection thresholds of 2.5 times the root mean square noise of event-free data epochs.

Extracellular electrophysiology

Acute hippocampal slices were prepared from mice deeply anesthetized with a 4:1 ketamine/xylazine solution (100 mg/kg, i.p.) and transcardially perfused (~30 mL, 30 mL/min) with cold (1-2 ºC) sucrose-based artificial cerebrospinal fluid (sucrose-aCSF) containing (in mM): NaCl (85), sucrose (75), $NaHCO_3$ (26), dextrose (25), KCl (3), $CaCl_2$ (2.5), NaH_2PO_4 (1.4), $MgSO_4$ (1.3) saturated with carbogen. The brain was extracted, cooled for an additional 60 seconds in sucrose-aCSF and then mounted horizontally (dorsal side down) to the cutting surface of a vibratome. We took the first three 400 µM thick sections starting approximately 1.2 mm beneath the ventral surface. The hippocampi and surrounding cortex were then dissected from the whole-brain sections and transferred to an interface-style holding chamber that contained normal aCSF at 24 °C. Extracellular recordings commenced at least 60 minutes thereafter in an interface-style recording chamber warmed to 33.5 °C. Local field potentials (LFP) were recorded using silver/silver-chloride electrodes in 2-4 MΩ borosilicate glass micropipettes backfilled with normal-aCSF. Signals were amplified (100 x) and bandpass-filtered (0.1 Hz - 3 kHz) using a differential amplifier. Records were digitized at 25 kHz using an analog-to-digital converter. Acquisition and offline analyses were performed using custom MATLAB scripts Power spectral density was estimated using 2^{13} point fast Fourier transforms applied to n = 1200, 250 ms Hanning-weighted data epochs segmented from five minute continuous recordings.

Immunohistochemistry

Mice were perfused with ice-cold 4% paraformaldehyde in 1 x PBS. Brains were removed, post-fixed overnight and equilibrated with 30% sucrose before cryostat sectioning. Free-floating coronal sections (40µm) were treated with blocking solution (0.2% Triton X-100, 5% normal

goat serum in 1 x PBS) for 2 hrs and incubated with primary antibody solution: mouse anti-HA (covance HA.11; 1:500) and Alexa-680 conjugated streptavidin (Jackson 016-620-084; 1:500) overnight at 4°C. After washing 3 times with PBS containing 0.2% Triton X-100, tissue was stained with goat anti-mouse Alexa 555 (LifeTechnology A- A21425; 1:500) and Alexa-680 conjugated streptavidin (1:500) overnight at 4°C. Following DAPI (Sigma D9542; 1:1000) staining, sections were washed 3 times in PBS containing 0.2% Triton X-100 and mounted onto the glass slides using FluorSave aqueous mounting medium. Images were taken with a Zeiss LSM 710. All configurations were equally set between samples.

Primary neuronal culture and immunocytochemistry

Primary neuronal cultures from mouse hippocampus were prepared as described previously (Carlson et al., 2011). Briefly, P0 pups were rapidly decapitated and hippocampal neurons were collected and plated onto poly-L-lysine-coated coverslips. Neurons were cultured in Neurobasal A medium supplemented with 2% (v/v) B-27 supplement and 1% (v/v) GlutaMAX. Neuronal transfections were performed with 2ug of DNA using Lipofectamine 2000 according to the manufacturer's instructions on DIV9 after plating. Samples were fixed at DIV13 in 4% PFA/4% sucrose in PBS for 5 min at 37°C. They were permeabilized and blocked with 0.2% Triton X-100 and 5% normal goat serum in 1x PBS at room temperature for 60 min. Samples were then incubated with primary antibodies: mouse anti-HA (covance HA.11; 1:500), mouse anti-Flag (Sigma F1804; 1:500), mouse anti-Myc (Sigma MABE282; 1:500) for 1hr at RT. After washing with 1 x PBS, samples were incubated with goat anti-mouse Alexa Fluor 555 (1:500) for 30min at room temperature. After washing 3 times, coverslips were mounted onto the glass slides and images were acquired using an oil immersion 63x Plan-Apochromat objective on a Zeiss LSM 710. For in vitro CRISPR mediated knock down experiments, hippocampal neurons were prepared from *Rosa26-LSL-Cas9* P0 pups and infected with AAV:*Cre/InSyn1:gRNA* virus or AAV:*Cre/ (-):gRNA* control virus at DIV4. At DIV16, neurons were fixed and stained with primary antibody solution: mouse anti-PSD-95 (ThermoFisher, MA1-046; 1:500), rabbit anti-$GABA_AR\gamma2$ (Synaptic Systems 224003; 1:500), mouse anti-alpha-dystroglycan (Millipore IIH6C4; 1:200), chicken anti-GFP (Abcam ab13970; 1:1000). Species specific secondary antibodies; goat anti-mouse Alexa 555 (1:500), goat anti-rabbit Alexa 647 (LT A31573; 1:500), goat anti-chicken Alexa 488 (LT A11039; 1:500) were incubated for 30min at RT. Samples were stained with DAPI, followed by 3 washes of PBS and mounted with mounting media. To re-express InSyn1, neurons were transfected with gRNA resistant HA-InSyn1 plasmid by Amaxa Nucleofection (Lonza, VPG) according to the manufacture's protocol at the day of plating. Mounted coverslips were imaged using 63x by Zeiss 710 confocal microscope with 488-, 561- and 633-nm lasers in Z-stack of 5 sections per image with 0.3µm depth and the consecutive 3 images were maximum projected. All the parameters taken by confocal microscopy were consistent between each images. The Puncta Analyzer plugin for ImageJ 1.29 was used to count the puncta number per image and the co-localized puncta (*61*). Background intensity was subtracted from the projected images (rolling ball radius = 50) and threshold to detect discrete puncta without introducing noise. Each puncta density was normalized by the area of GFP positive neurons. To calculate the percentage of colocalizing pixels between GPHN.FingR-GFP and exogenous expressed iPSD proteins, dendritic segments with recognizable clusters were outlined and saved as region of interest (ROI). The image calculator tool of ImageJ was used to measure the overlapping area between channels in each ROI.

Data and Statistical Analyses

Statistical comparisons were performed in Microsoft Excel or SPSS using independent-samples t-tests or one-way ANOVAs. Significant F-values were followed by Tukey's post-hoc tests. Assumptions of normality and error variance homogeneity were first tested using Shapiro-Wilks and Levene's tests, respectively. If error variance violations could not be corrected by log-transformations, statistical comparisons were made using non-parametric test equivalents (i.e. Mann-Whitney or Kruskal-Wallis tests). Alpha values were set at 0.05 for all tests. Summary values presented in the text represent mean ± SEM, unless indicated otherwise.

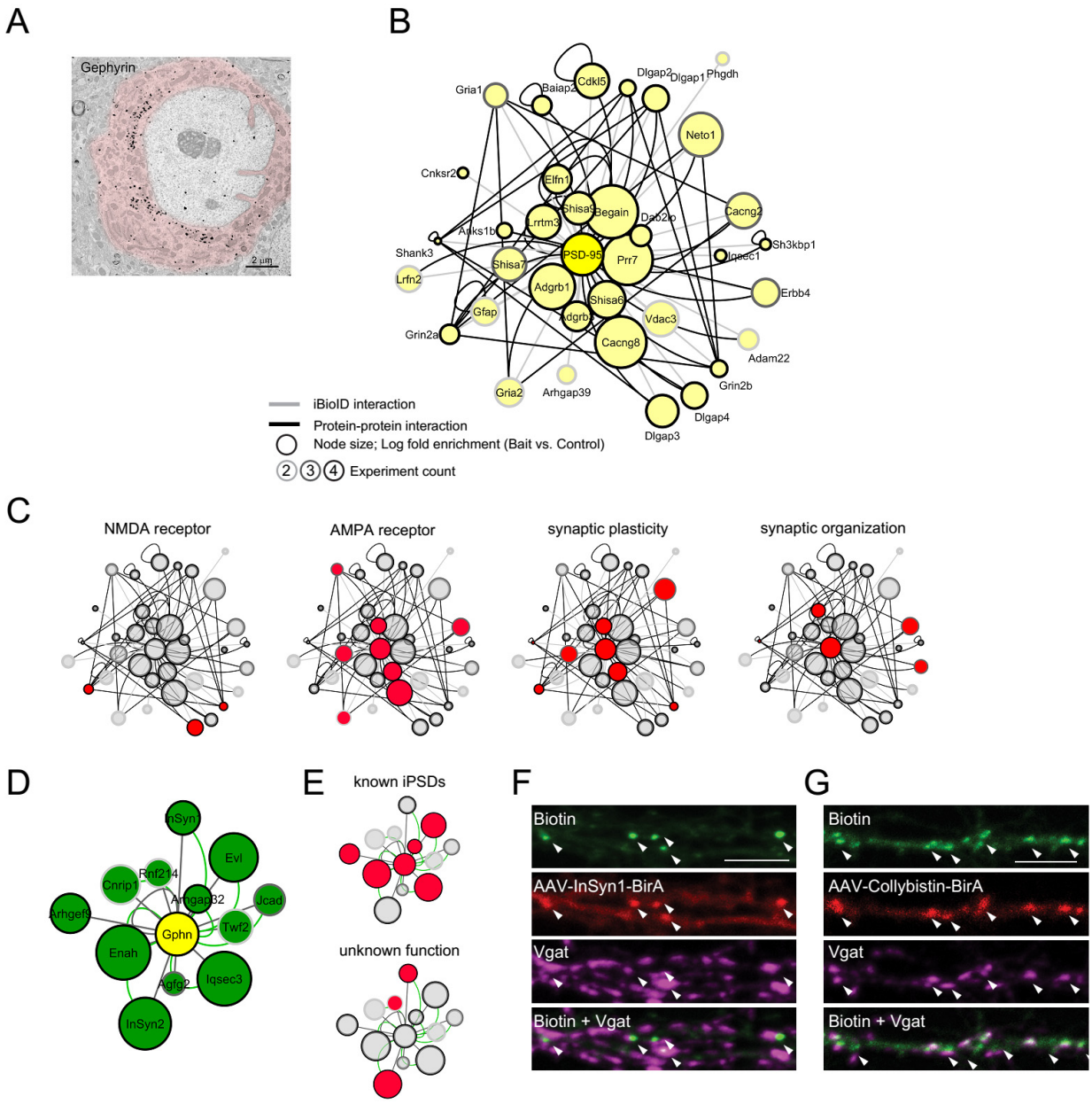

Fig. S1. iBioID characterization and initial proteome networks and validation of iPSD BirA-fusion proteins. A, Electron micrograph showing gold bead streptavidin labeling of non-specific biotinylation in Golgi, mitochondria, and nucleus of cell body of a neuron in the cortex from a BirA-gephyrin infected mouse. Scale bar, 2 µm. Network analysis of enriched proteins from (**A-B**) PSD-95–BirA or (**C-D**) BirA-gephyrin iBioID by semi-quantitative mass spectrometry analysis. Four biological samples from each BirA-gephyrin, PSD-95–BirA and BirA probe were analyzed using a Synapt G2 mass spectrometer. Acquired protein spectral counts were used to calculate iBAQ score for each identified protein. The enriched proteins in PSD-95 or gephyrin fractions were considered specific at levels 2-fold (PSD-95) or 2.5-fold (gephyrin) higher than control fractions based on iBAQ scores. **B & D,** Clustergrams showing the locations of (B) PSD proteins and (D) iPSD proteins in selected functional categories. To expand the iBioID proteome analysis for the inhibitory synaptic complex, (**E**) collybistin-BirA or

(**F**) InSyn1-BirA was expressed in cultured hippocampal neurons and co-stained with inhibitory pre-synaptic marker, Vgat to demonstrate their localization. Scale bar, 5 μm.

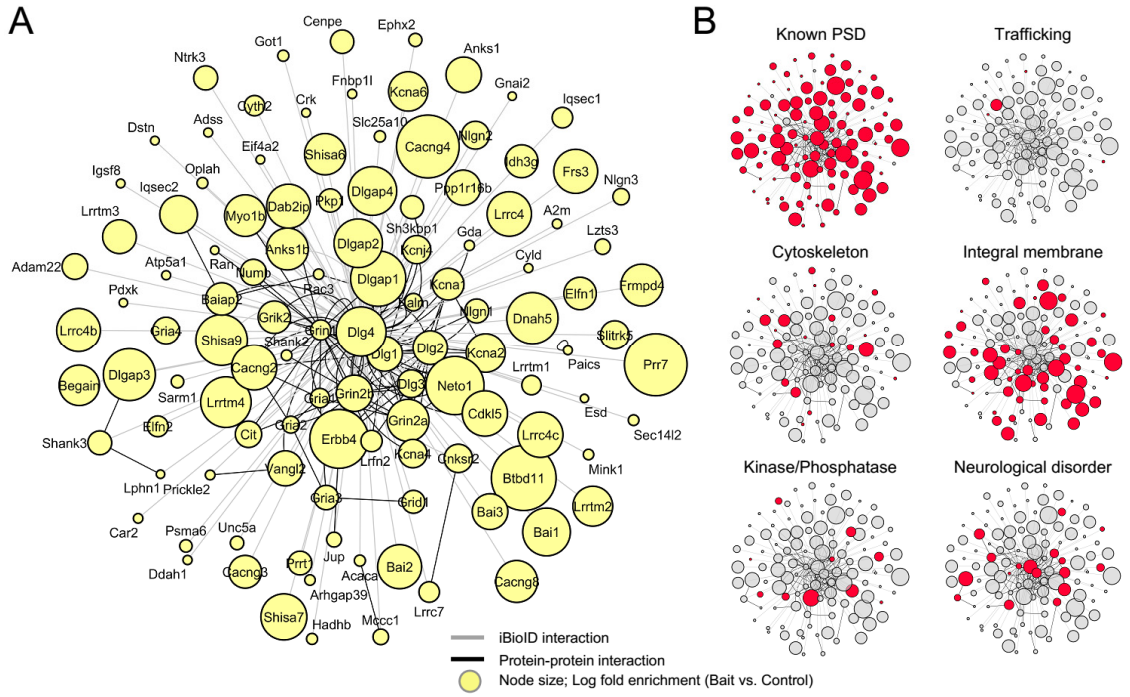

Fig. S2: PSD-95 iBioID network. A, PSD-95–BirA identifies a network of excitatory synaptic proteins from mouse brain. Node titles correspond to gene name and size represents fold-enrichment values over negative control. Edges are shaded according to the types of interactions (grey, iBioID; black, Protein-Protein interactions previously reported). **B**, Clustergrams depicting the positions of synaptic proteins (red) in selected functional categories.

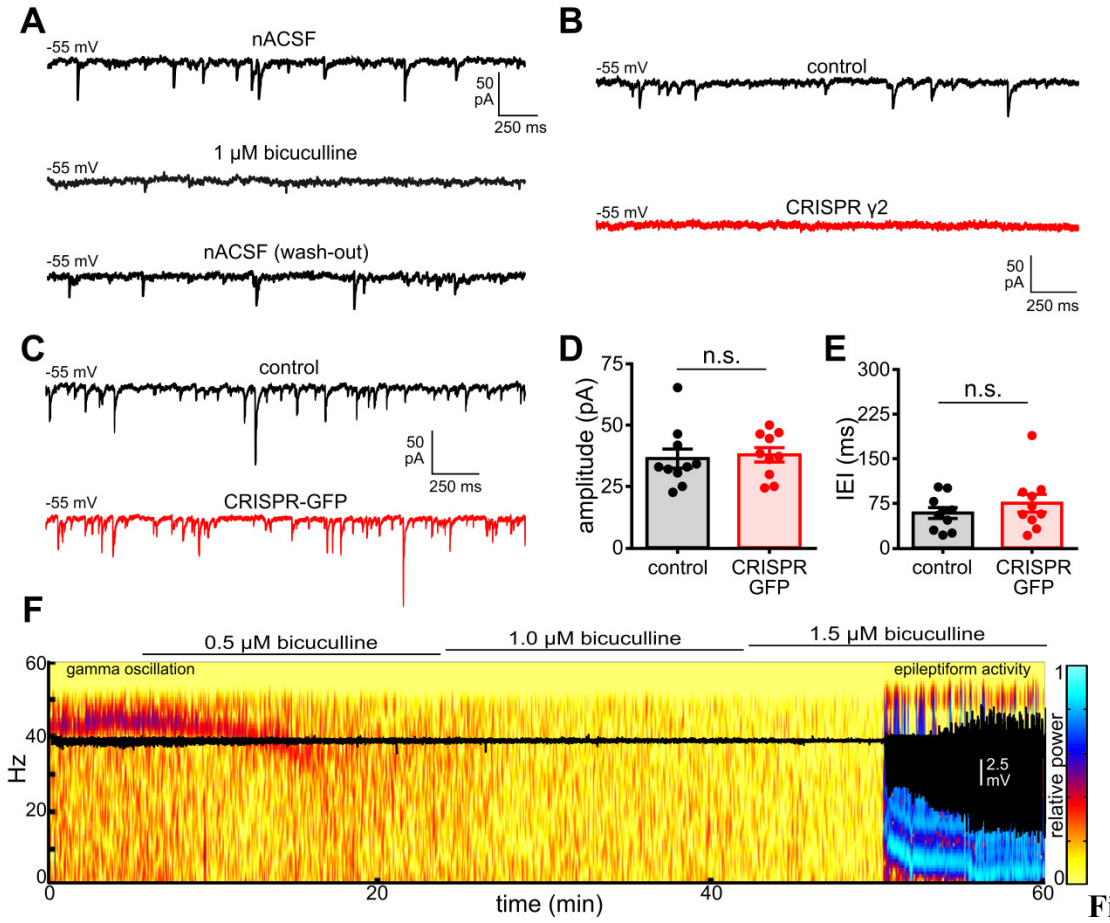

Fig. S3. Validation of CRISPR-mediated depletion approach for mIPSC analysis. A, KCl-filled patch pipettes were used to record $GABA_A$-dependent miniature inhibitory postsynaptic currents ($GABA_A$ mIPSCs) from CA1 pyramidal cells in the presence of extracellular medium containing 1 µM tetrodotoxin and glutamatergic antagonists (20 µM CNQX, 50 µM APV). $GABA_A$ mIPSCs appeared as negative-going currents at –55 mV holding potentials and were reversibly sensitive to bicuculline ($GABA_A$ receptor antagonist, n = 3). **B**, Electrophysiological validation of CRISPR technique for mIPSC analysis by targeting the critical γ2 subunit of the $GABA_A$ receptor. Traces compare epochs of spontaneous activity recorded from a control neuron (*black trace*) and a γ2 KO neuron (*red trace*) at –55 mV holding potentials. $GABA_A$ mIPSCs were prominent in the control cells but absent in the γ2 KO cells (n = 3 cell pairs). **C**, $GABA_A$ mIPSCs recorded from a control cell (*black trace*) and GFP-transfected cell (*red trace*). Biolistic transfection did not significantly alter **D**, median current amplitude (percent difference = 1.5%, $t_{18} = 0.31$, $p = 0.76$) or **E**, median current inter-event interval (IEI) (percent difference = 16.6%, $t_{18} = 0.94$, $p = 0.36$). **F**, Network hyperexcitability in a WT slice following GABAergic attenuation. The pseudocolor time-frequency plot shows signal power during wash-in of 0.5 µM bicuculline steps, which transitioned a carbachol-induced gamma oscillation (20-50 Hz activity) into epileptiform bursts (DC-15 Hz activity), Such hyperexcitable activity was seen in InSyn1 depleted slices in the absence of GABA-A receptor antagonism.

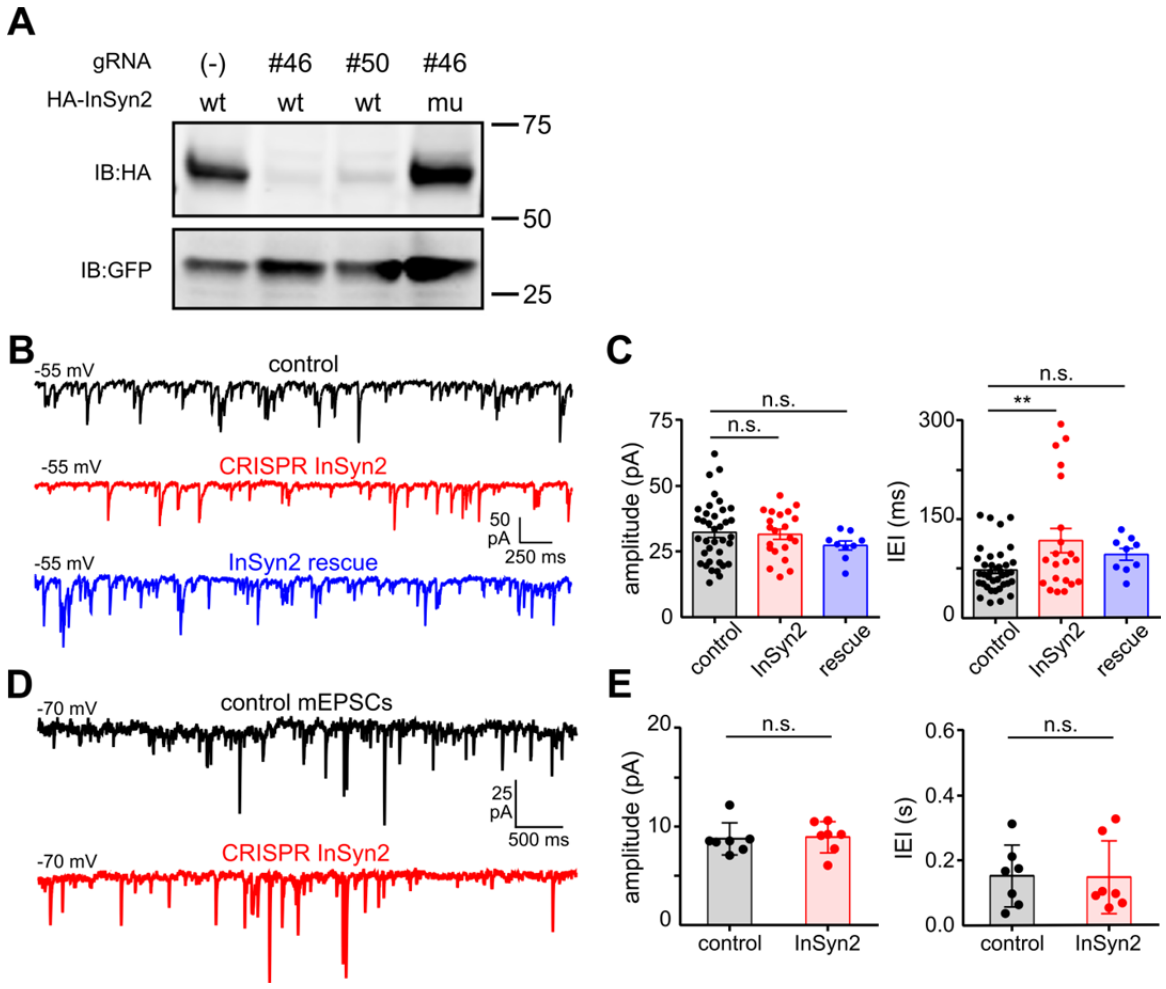

Fig. S4. CRISPR-mediated depletion of InSyn2. A, Validation of InSyn2 gRNA and rescue constructs by 293T co-transfection and immunoblotting. **B,** $GABA_A$-dependent miniature inhibitory postsynaptic currents ($GABA_A$ mIPSCs) recorded from CA1 pyramidal cells (control—*black*, InSyn2—*red*, rescue—*blue*). **C,** InSyn2 depletion significantly increased inter-event intervals of $GABA_A$ mIPSCs without affecting current amplitudes. **D,** AMPAR-dependent miniature EPSCs characteristics are not altered in InSyn2 depleted neurons. **p < 0.01.

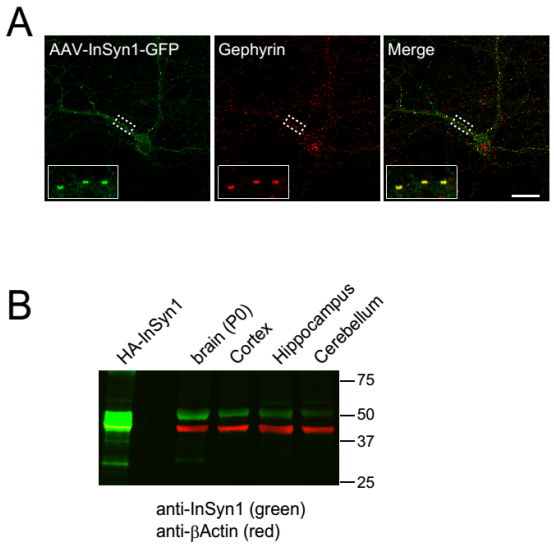

Fig. S5. Analysis of InSyn1-GFP and α-InSyn1 polyclonal antibody. A, Hippocampal neurons were transduced with AAV InSyn1-GFP, and were co-stained with gephyrin. Scale bar, 20 μm. **B**, Western blot analysis of endogenous InSyn1 expression (*green*) in P0 or P90 mouse brain lysates from different regions along with exogenously expressed HA-InSyn1 (*red*) using affinity purified polyclonal antibody against InSyn1.

Excel tables

Table S1: Filtered proteins based on EM staining
Table S2: Enriched biotinylated proteins from iBioID pilot
Table S3: Enriched biotinylated proteins from PSD-95–BirA probe utilizing quantitative mass spectrometry analysis
Table S4: Enriched biotinylated proteins from three independent iPSD targeted BirA probes
Table S5: Proteins common to ePSD and iPSD datasets
Table S6: InSyn1 GFP-trap data

References and Notes

1. E. G. Gray, Axo-somatic and axo-dendritic synapses of the cerebral cortex: An electron microscope study. *J. Anat.* **93**, 420–433 (1959). Medline

2. R. C. Malenka, M. F. Bear, LTP and LTD: An embarrassment of riches. *Neuron* **44**, 5–21 (2004). Medline doi:10.1016/j.neuron.2004.09.012

3. M. B. Kennedy, H. C. Beale, H. J. Carlisle, L. R. Washburn, Integration of biochemical signalling in spines. *Nat. Rev. Neurosci.* **6**, 423–434 (2005). Medline doi:10.1038/nrn1685

4. S. G. Grant, Synaptopathies: Diseases of the synaptome. *Curr. Opin. Neurobiol.* **22**, 522–529 (2012). Medline doi:10.1016/j.conb.2012.02.002

5. L. Volk, S. L. Chiu, K. Sharma, R. L. Huganir, Glutamate synapses in human cognitive disorders. *Annu. Rev. Neurosci.* **38**, 127–149 (2015). Medline doi:10.1146/annurev-neuro-071714-033821

6. K. J. Roux, D. I. Kim, M. Raida, B. Burke, A promiscuous biotin ligase fusion protein identifies proximal and interacting proteins in mammalian cells. *J. Cell Biol.* **196**, 801–810 (2012). Medline doi:10.1083/jcb.201112098

7. D. I. Kim, B. Kc, W. Zhu, K. Motamedchaboki, V. Doye, K. J. Roux, Probing nuclear pore complex architecture with proximity-dependent biotinylation. *Proc. Natl. Acad. Sci. U.S.A.* **111**, E2453–E2461 (2014). Medline doi:10.1073/pnas.1406459111

8. Z. Yao, J. Petschnigg, R. Ketteler, I. Stagljar, Application guide for omics approaches to cell signaling. *Nat. Chem. Biol.* **11**, 387–397 (2015). Medline doi:10.1038/nchembio.1809

9. A. Poulopoulos, G. Aramuni, G. Meyer, T. Soykan, M. Hoon, T. Papadopoulos, M. Zhang, I. Paarmann, C. Fuchs, K. Harvey, P. Jedlicka, S. W. Schwarzacher, H. Betz, R. J. Harvey, N. Brose, W. Zhang, F. Varoqueaux, Neuroligin 2 drives postsynaptic assembly at perisomatic inhibitory synapses through gephyrin and collybistin. *Neuron* **63**, 628–642 (2009). Medline doi:10.1016/j.neuron.2009.08.023

10. S. K. Tyagarajan, J. M. Fritschy, Gephyrin: A master regulator of neuronal function? *Nat. Rev. Neurosci.* **15**, 141–156 (2014). Medline doi:10.1038/nrn3670

11. P. Prior, B. Schmitt, G. Grenningloh, I. Pribilla, G. Multhaup, K. Beyreuther, Y. Maulet, P. Werner, D. Langosch, J. Kirsch, H. Betz, Primary structure and alternative splice variants of gephyrin, a putative glycine receptor-tubulin linker protein. *Neuron* **8**, 1161–1170 (1992). Medline doi:10.1016/0896-6273(92)90136-2

12. J. W. Um, G. Choii, D. Park, D. Kim, S. Jeon, H. Kang, T. Mori, T. Papadopoulos, T. Yoo, Y. Lee, E. Kim, K. Tabuchi, J. Ko, IQ motif and SEC7 domain-containing protein 3 (IQSEC3) interacts with gephyrin to promote inhibitory synapse formation. *J. Biol. Chem.* **291**, 10119–10130 (2016). Medline doi:10.1074/jbc.M115.712893

13. Known iPSD proteins included eight $GABA_A$ receptor subunits, inhibitory transmembrane adhesion proteins [e.g., neuroligin-2 (*33*–*35*), Slitrk3 (*36*), and

neuroplastin (*37*, *38*)], as well as signaling- and actin-associated proteins, such as Trim3 (*39*), Enah (*40*), profiling (*41*); and dystrophin complex proteins (including alpha-1-syntrophin, dystrobrevin alpha, and dystrophin) (*42*).

14. G. G. Gross, J. A. Junge, R. J. Mora, H. B. Kwon, C. A. Olson, T. T. Takahashi, E. R. Liman, G. C. Ellis-Davies, A. W. McGee, B. L. Sabatini, R. W. Roberts, D. B. Arnold, Recombinant probes for visualizing endogenous synaptic proteins in living neurons. *Neuron* **78**, 971–985 (2013). Medline doi:10.1016/j.neuron.2013.04.017

15. S. Incontro, C. S. Asensio, R. H. Edwards, R. A. Nicoll, Efficient, complete deletion of synaptic proteins using CRISPR. *Neuron* **83**, 1051–1057 (2014). Medline doi:10.1016/j.neuron.2014.07.043

16. E. O. Mann, J. M. Suckling, N. Hajos, S. A. Greenfield, O. Paulsen, Perisomatic feedback inhibition underlies cholinergically induced fast network oscillations in the rat hippocampus in vitro. *Neuron* **45**, 105–117 (2005). Medline doi:10.1016/j.neuron.2004.12.016

17. R. J. Platt, S. Chen, Y. Zhou, M. J. Yim, L. Swiech, H. R. Kempton, J. E. Dahlman, O. Parnas, T. M. Eisenhaure, M. Jovanovic, D. B. Graham, S. Jhunjhunwala, M. Heidenreich, R. J. Xavier, R. Langer, D. G. Anderson, N. Hacohen, A. Regev, G. Feng, P. A. Sharp, F. Zhang, CRISPR-Cas9 knockin mice for genome editing and cancer modeling. *Cell* **159**, 440–455 (2014). Medline doi:10.1016/j.cell.2014.09.014

18. M. Pane, S. Messina, C. Bruno, A. D'Amico, M. Villanova, B. Brancalion, S. Sivo, F. Bianco, P. Striano, D. Battaglia, D. Lettori, G. L. Vita, E. Bertini, F. Gualandi, V. Ricotti, A. Ferlini, E. Mercuri, Duchenne muscular dystrophy and epilepsy. *Neuromuscul. Disord.* **23**, 313–315 (2013). Medline doi:10.1016/j.nmd.2013.01.011

19. E. A. Heller, W. Zhang, F. Selimi, J. C. Earnheart, M. A. Ślimak, J. Santos-Torres, I. Ibañez-Tallon, C. Aoki, B. T. Chait, N. Heintz, The biochemical anatomy of cortical inhibitory synapses. *PLOS ONE* **7**, e39572 (2012). Medline doi:10.1371/journal.pone.0039572

20. Y. Kang, Y. Ge, R. M. Cassidy, V. Lam, L. Luo, K. M. Moon, R. Lewis, R. S. Molday, R. O. Wong, L. J. Foster, A. M. Craig, A combined transgenic proteomic analysis and regulated trafficking of neuroligin-2. *J. Biol. Chem.* **289**, 29350–29364 (2014). Medline doi:10.1074/jbc.M114.549279

21. Y. Nakamura, D. H. Morrow, A. Modgil, D. Huyghe, T. Z. Deeb, M. J. Lumb, P. A. Davies, S. J. Moss, Proteomic characterization of inhibitory synapses using a novel pHluorin-tagged. *J. Biol. Chem.* **291**, 12394–12407 (2016). Medline doi:10.1074/jbc.M116.724443

22. S. Sugita, F. Saito, J. Tang, J. Satz, K. Campbell, T. C. Südhof, A stoichiometric complex of neurexins and dystroglycan in brain. *J. Cell Biol.* **154**, 435–446 (2001). Medline doi:10.1083/jcb.200105003

23. D. E. Michele, R. Barresi, M. Kanagawa, F. Saito, R. D. Cohn, J. S. Satz, J. Dollar, I. Nishino, R. I. Kelley, H. Somer, V. Straub, K. D. Mathews, S. A. Moore, K. P.

Campbell, Post-translational disruption of dystroglycan-ligand interactions in congenital muscular dystrophies. *Nature* **418**, 417–421 (2002). Medline doi:10.1038/nature00837

24. K. L. Villa, K. P. Berry, J. Subramanian, J. W. Cha, W. C. Oh, H. B. Kwon, Y. Kubota, P. T. So, E. Nedivi, Inhibitory synapses are repeatedly assembled and removed at persistent sites in vivo. *Neuron* **89**, 756–769 (2016). Medline doi:10.1016/j.neuron.2016.01.010

25. J. N. Bourne, K. M. Harris, Coordination of size and number of excitatory and inhibitory synapses results in a balanced structural plasticity along mature hippocampal CA1 dendrites during LTP. *Hippocampus* **21**, 354–373 (2011). Medline doi:10.1002/hipo.20768

26. I. Lushnikova, G. Skibo, D. Muller, I. Nikonenko, Excitatory synaptic activity is associated with a rapid structural plasticity of inhibitory synapses on hippocampal CA1 pyramidal cells. *Neuropharmacology* **60**, 757–764 (2011). Medline doi:10.1016/j.neuropharm.2010.12.014

27. F. Niwa, H. Bannai, M. Arizono, K. Fukatsu, A. Triller, K. Mikoshiba, Gephyrin-independent GABA(A)R mobility and clustering during plasticity. *PLOS ONE* **7**, e36148 (2012). Medline doi:10.1371/journal.pone.0036148

28. B. Dejanovic, M. Semtner, S. Ebert, T. Lamkemeyer, F. Neuser, B. Lüscher, J. C. Meier, G. Schwarz, Palmitoylation of gephyrin controls receptor clustering and plasticity of GABAergic synapses. *PLOS Biol.* **12**, e1001908 (2014). Medline doi:10.1371/journal.pbio.1001908

29. E. M. Petrini, T. Ravasenga, T. J. Hausrat, G. Iurilli, U. Olcese, V. Racine, J. B. Sibarita, T. C. Jacob, S. J. Moss, F. Benfenati, P. Medini, M. Kneussel, A. Barberis, Synaptic recruitment of gephyrin regulates surface GABAA receptor dynamics for the expression of inhibitory LTP. *Nat. Commun.* **5**, 3921 (2014). Medline doi:10.1038/ncomms4921

30. C. E. Flores, I. Nikonenko, P. Mendez, J. M. Fritschy, S. K. Tyagarajan, D. Muller, Activity-dependent inhibitory synapse remodeling through gephyrin phosphorylation. *Proc. Natl. Acad. Sci. U.S.A.* **112**, E65–E72 (2015). Medline doi:10.1073/pnas.1411170112

31. J. L. Chen, K. L. Villa, J. W. Cha, P. T. So, Y. Kubota, E. Nedivi, Clustered dynamics of inhibitory synapses and dendritic spines in the adult neocortex. *Neuron* **74**, 361–373 (2012). Medline doi:10.1016/j.neuron.2012.02.030

32. D. van Versendaal, R. Rajendran, M. H. Saiepour, J. Klooster, L. Smit-Rigter, J. P. Sommeijer, C. I. De Zeeuw, S. B. Hofer, J. A. Heimel, C. N. Levelt, Elimination of inhibitory synapses is a major component of adult ocular dominance plasticity. *Neuron* **74**, 374–383 (2012). Medline doi:10.1016/j.neuron.2012.03.015

33. F. Varoqueaux, S. Jamain, N. Brose, Neuroligin 2 is exclusively localized to inhibitory synapses. *Eur. J. Cell Biol.* **83**, 449–456 (2004). Medline doi:10.1078/0171-9335-00410

34. E. R. Graf, X. Zhang, S. X. Jin, M. W. Linhoff, A. M. Craig, Neurexins induce differentiation of GABA and glutamate postsynaptic specializations via neuroligins. *Cell* **119**, 1013–1026 (2004). Medline doi:10.1016/j.cell.2004.11.035

35. B. Chih, H. Engelman, P. Scheiffele, Control of excitatory and inhibitory synapse formation by neuroligins. *Science* **307**, 1324–1328 (2005). Medline doi:10.1126/science.1107470

36. H. Takahashi, K. Katayama, K. Sohya, H. Miyamoto, T. Prasad, Y. Matsumoto, M. Ota, H. Yasuda, T. Tsumoto, J. Aruga, A. M. Craig, Selective control of inhibitory synapse development by Slitrk3-PTP δ trans synaptic interaction. *Nat. Neurosci.* **15**, 389–398, S1–S2 (2012). Medline doi:10.1038/nn.3040

37. P. W. Beesley, R. Herrera-Molina, K. H. Smalla, C. Seidenbecher, The neuroplastin adhesion molecules: Key regulators of neuronal plasticity and synaptic function. *J. Neurochem.* **131**, 268–283 (2014). Medline doi:10.1111/jnc.12816

38. R. Herrera-Molina, I. Sarto-Jackson, C. Montenegro-Venegas, M. Heine, K. H. Smalla, C. I. Seidenbecher, P. W. Beesley, E. D. Gundelfinger, D. Montag, Structure of excitatory synapses and $GABA_A$ receptor localization at inhibitory synapses are regulated by neuroplastin-65. *J. Biol. Chem.* **289**, 8973–8988 (2014). Medline doi:10.1074/jbc.M113.514992

39. C. C. Cheung, C. Yang, T. Berger, K. Zaugg, P. Reilly, A. J. Elia, A. Wakeham, A. You-Ten, N. Chang, L. Li, Q. Wan, T. W. Mak, Identification of BERP (brain-expressed RING finger protein) as a p53 target gene that modulates seizure susceptibility through interacting with GABA(A) receptors. *Proc. Natl. Acad. Sci. U.S.A.* **107**, 11883–11888 (2010). Medline doi:10.1073/pnas.1006529107

40. T. Giesemann, G. Schwarz, R. Nawrotzki, K. Berhörster, M. Rothkegel, K. Schlüter, N. Schrader, H. Schindelin, R. R. Mendel, J. Kirsch, B. M. Jockusch, Complex formation between the postsynaptic scaffolding protein gephyrin, profilin, and Mena: A possible link to the microfilament system. *J. Neurosci.* **23**, 8330–8339 (2003). Medline

41. K. Murk, N. Wittenmayer, K. Michaelsen-Preusse, T. Dresbach, C. A. Schoenenberger, M. Korte, B. M. Jockusch, M. Rothkegel, Neuronal profilin isoforms are addressed by different signalling pathways. *PLOS ONE* **7**, e34167 (2012). Medline doi:10.1371/journal.pone.0034167

42. G. S. Pilgram, S. Potikanond, R. A. Baines, L. G. Fradkin, J. N. Noordermeer, The roles of the dystrophin-associated glycoprotein complex at the synapse. *Mol. Neurobiol.* **41**, 1–21 (2010). Medline doi:10.1007/s12035-009-8089-5

43. N. Akshoomoff, S. N. Mattson, P. D. Grossfeld, Evidence for autism spectrum disorder in Jacobsen syndrome: Identification of a candidate gene in distal 11q. *Genet. Med.* **17**, 143–148 (2015). Medline doi:10.1038/gim.2014.86

44. A. S. Allen, S. F. Berkovic, P. Cossette, N. Delanty, D. Dlugos, E. E. Eichler, M. P. Epstein, T. Glauser, D. B. Goldstein, Y. Han, E. L. Heinzen, Y. Hitomi, K. B. Howell, M. R. Johnson, R. Kuzniecky, D. H. Lowenstein, Y. F. Lu, M. R. Madou, A. G. Marson, H. C. Mefford, S. Esmaeeli Nieh, T. J. O'Brien, R. Ottman, S. Petrovski, A. Poduri, E. K. Ruzzo, I. E. Scheffer, E. H. Sherr, C. J. Yuskaitis, B. Abou-Khalil, B. K. Alldredge, J. F. Bautista, S. F. Berkovic, A. Boro, G. D. Cascino, D. Consalvo, P. Crumrine, O. Devinsky, D. Dlugos, M. P. Epstein, M. Fiol, N. B. Fountain, J. French, D. Friedman, E. B. Geller, T. Glauser, S. Glynn, S. R. Haut, J. Hayward, S. L. Helmers, S. Joshi, A. Kanner, H. E. Kirsch, R. C. Knowlton, E. H. Kossoff, R. Kuperman, R. Kuzniecky, D. H. Lowenstein, S. M. McGuire, P. V. Motika, E. J. Novotny, R. Ottman, J. M. Paolicchi, J. M. Parent, K. Park, A. Poduri, I. E. Scheffer, R. A. Shellhaas, E. H. Sherr, J. J. Shih, R. Singh, J. Sirven, M. C. Smith, J. Sullivan, L. Lin Thio, A. Venkat, E. P. Vining, G. K. Von Allmen, J. L. Weisenberg, P. Widdess-Walsh, M. R. WinawerEpi4K ConsortiumEpilepsy Phenome/Genome Project, De novo mutations in epileptic encephalopathies. *Nature* **501**, 217–221 (2013). Medline doi:10.1038/nature12439

45. L. S. Weaving, J. Christodoulou, S. L. Williamson, K. L. Friend, O. L. McKenzie, H. Archer, J. Evans, A. Clarke, G. J. Pelka, P. P. Tam, C. Watson, H. Lahooti, C. J. Ellaway, B. Bennetts, H. Leonard, J. Gécz, Mutations of CDKL5 cause a severe neurodevelopmental disorder with infantile spasms and mental retardation. *Am. J. Hum. Genet.* **75**, 1079–1093 (2004). Medline doi:10.1086/426462

46. S. Fehr, M. Wilson, J. Downs, S. Williams, A. Murgia, S. Sartori, M. Vecchi, G. Ho, R. Polli, S. Psoni, X. Bao, N. de Klerk, H. Leonard, J. Christodoulou, The CDKL5 disorder is an independent clinical entity associated with early-onset encephalopathy. *Eur. J. Hum. Genet.* **21**, 266–273 (2013). Medline doi:10.1038/ejhg.2012.156

47. A. Falace, F. Filipello, V. La Padula, N. Vanni, F. Madia, D. De Pietri Tonelli, F. A. de Falco, P. Striano, F. Dagna Bricarelli, C. Minetti, F. Benfenati, A. Fassio, F. Zara, TBC1D24, an ARF6-interacting protein, is mutated in familial infantile myoclonic epilepsy. *Am. J. Hum. Genet.* **87**, 365–370 (2010). Medline doi:10.1016/j.ajhg.2010.07.020

48. A. U. Rehman, R. L. Santos-Cortez, R. J. Morell, M. C. Drummond, T. Ito, K. Lee, A. A. Khan, M. A. Basra, N. Wasif, M. Ayub, R. A. Ali, S. I. Raza, D. A. Nickerson, J. Shendure, M. Bamshad, S. Riazuddin, N. Billington, S. N. Khan, P. L. Friedman, A. J. Griffith, W. Ahmad, S. Riazuddin, S. M. Leal, T. B. Friedman; University of Washington Center for Mendelian Genomics, Mutations in TBC1D24, a gene associated with epilepsy, also cause nonsyndromic deafness DFNB86. *Am. J. Hum. Genet.* **94**, 144–152 (2014). Medline doi:10.1016/j.ajhg.2013.12.004

49. M. D. Shirley, H. Tang, C. J. Gallione, J. D. Baugher, L. P. Frelin, B. Cohen, P. E. North, D. A. Marchuk, A. M. Comi, J. Pevsner, Sturge-Weber syndrome and port-wine stains caused by somatic mutation in GNAQ. *N. Engl. J. Med.* **368**, 1971–1979 (2013). Medline doi:10.1056/NEJMoa1213507

50. S. Quéméner-Redon, C. Bénech, S. Audebert-Bellanger, G. Friocourt, M. Planes, P. Parent, C. Férec, A small de novo 16q24.1 duplication in a woman with severe clinical features. *Eur. J. Med. Genet.* **56**, 211–215 (2013). Medline doi:10.1016/j.ejmg.2013.01.001

51. L. Basel-Vanagaite, R. Attia, M. Yahav, R. J. Ferland, L. Anteki, C. A. Walsh, T. Olender, R. Straussberg, N. Magal, E. Taub, V. Drasinover, A. Alkelai, D. Bercovich, G. Rechavi, A. J. Simon, M. Shohat, The CC2D1A, a member of a new gene family with C2 domains, is involved in autosomal recessive non-syndromic mental retardation. *J. Med. Genet.* **43**, 203–210 (2006). Medline doi:10.1136/jmg.2005.035709

52. A. Mory, E. Dagan, B. Illi, P. Duquesnoy, S. Mordechai, I. Shahor, S. Romani, N. Hawash-Moustafa, H. Mandel, E. M. Valente, S. Amselem, R. Gershoni-Baruch, A nonsense mutation in the human homolog of *Drosophila rogdi* causes Kohlschutter-Tonz syndrome. *Am. J. Hum. Genet.* **90**, 708–714 (2012). Medline doi:10.1016/j.ajhg.2012.03.005

53. A. Schossig, N. I. Wolf, C. Fischer, M. Fischer, G. Stocker, S. Pabinger, A. Dander, B. Steiner, O. Tönz, D. Kotzot, E. Haberlandt, A. Amberger, B. Burwinkel, K. Wimmer, C. Fauth, C. Grond-Ginsbach, M. J. Koch, A. Deichmann, C. von Kalle, C. R. Bartram, A. Kohlschütter, Z. Trajanoski, J. Zschocke, Mutations in *ROGDI* cause Kohlschütter-Tönz Syndrome. *Am. J. Hum. Genet.* **90**, 701–707 (2012). Medline doi:10.1016/j.ajhg.2012.02.012

54. G. Feng, H. Tintrup, J. Kirsch, M. C. Nichol, J. Kuhse, H. Betz, J. R. Sanes, Dual requirement for gephyrin in glycine receptor clustering and molybdoenzyme activity. *Science* **282**, 1321–1324 (1998). Medline doi:10.1126/science.282.5392.1321

55. N. H. Tomioka, H. Yasuda, H. Miyamoto, M. Hatayama, N. Morimura, Y. Matsumoto, T. Suzuki, M. Odagawa, Y. S. Odaka, Y. Iwayama, J. Won Um, J. Ko, Y. Inoue, S. Kaneko, S. Hirose, K. Yamada, T. Yoshikawa, K. Yamakawa, J. Aruga, Elfn1 recruits presynaptic mGluR7 in trans and its loss results in seizures. *Nat. Commun.* **5**, 4501 (2014). Medline doi:10.1038/ncomms5501

56. F. Nakatsu, M. Okada, F. Mori, N. Kumazawa, H. Iwasa, G. Zhu, Y. Kasagi, H. Kamiya, A. Harada, K. Nishimura, A. Takeuchi, T. Miyazaki, M. Watanabe, S. Yuasa, T. Manabe, K. Wakabayashi, S. Kaneko, T. Saito, H. Ohno, Defective function of GABA-containing synaptic vesicles in mice lacking the AP-3B clathrin adaptor. *J. Cell Biol.* **167**, 293–302 (2004). Medline doi:10.1083/jcb.200405032

57. A. Uezu, H. Okada, H. Murakoshi, C. D. del Vescovo, R. Yasuda, D. Diviani, S. H. Soderling, Modified SH2 domain to phototrap and identify phosphotyrosine proteins from subcellular sites within cells. *Proc. Natl. Acad. Sci. U.S.A.* **109**, E2929–E2938 (2012). Medline doi:10.1073/pnas.1207358109

58. I. H. Kim, M. A. Rossi, D. K. Aryal, B. Racz, N. Kim, A. Uezu, F. Wang, W. C. Wetsel, R. J. Weinberg, H. Yin, S. H. Soderling, Spine pruning drives antipsychotic-sensitive locomotion via circuit control of striatal dopamine. *Nat. Neurosci.* **18**, 883–891 (2015). Medline doi:10.1038/nn.4015

59. I. H. Kim, B. Racz, H. Wang, L. Burianek, R. Weinberg, R. Yasuda, W. C. Wetsel, S. H. Soderling, Disruption of Arp2/3 results in asymmetric structural plasticity of dendritic spines and progressive synaptic and behavioral abnormalities. *J. Neurosci.* **33**, 6081–6092 (2013). Medline doi:10.1523/JNEUROSCI.0035-13.2013

60. R. S. Westphal, S. H. Soderling, N. M. Alto, L. K. Langeberg, J. D. Scott, Scar/WAVE-1, a Wiskott-Aldrich syndrome protein, assembles an actin-associated multi-kinase scaffold. *EMBO J.* **19**, 4589–4600 (2000). Medline doi:10.1093/emboj/19.17.4589

61. W. C. Risher, S. Patel, I. H. Kim, A. Uezu, S. Bhagat, D. K. Wilton, L. J. Pilaz, J. Singh Alvarado, O. Y. Calhan, D. L. Silver, B. Stevens, N. Calakos, S. H. Soderling, C. Eroglu, Astrocytes refine cortical connectivity at dendritic spines. *eLife* **3**, 10.7554/eLife.04047 (2014). Medline doi:10.7554/eLife.04047